



Kinetics of nickel silicide growth in silicon nanowires: From linear to square root growth

Y. E. Yaish, A. Katsman, G. M. Cohen, and M. Beregovsky

Citation: *J. Appl. Phys.* **109**, 094303 (2011); doi: 10.1063/1.3574650

View online: <http://dx.doi.org/10.1063/1.3574650>

View Table of Contents: <http://jap.aip.org/resource/1/JAPIAU/v109/i9>

Published by the [American Institute of Physics](#).

Related Articles

Faster radial strain relaxation in InAs–GaAs core–shell heterowires

J. Appl. Phys. **111**, 044301 (2012)

Controlling domain walls velocities in ferromagnetic ring-shaped nanowires

Appl. Phys. Lett. **100**, 072405 (2012)

Manganese dioxide modified silicon nanowires and their excellent catalysis in the decomposition of methylene blue

Appl. Phys. Lett. **100**, 063104 (2012)

Growth and photoluminescence of self-catalyzed GaP/GaNP core/shell nanowires on Si(111) by gas source molecular beam epitaxy

Appl. Phys. Lett. **100**, 053108 (2012)

n-ZnO:N/p-Si nanowire photodiode prepared by atomic layer deposition

Appl. Phys. Lett. **100**, 041117 (2012)

Additional information on *J. Appl. Phys.*


Journal Homepage: <http://jap.aip.org/>

Journal Information: http://jap.aip.org/about/about_the_journal

Top downloads: http://jap.aip.org/features/most_downloaded

Information for Authors: <http://jap.aip.org/authors>

ADVERTISEMENT

	Working @ low temperatures? Contact Janis for Cryogenic Research Equipment Click here to browse our site at www.janis.com	
---	--	---

Kinetics of nickel silicide growth in silicon nanowires: From linear to square root growth

Y. E. Yaish,^{1,a)} A. Katsman,² G. M. Cohen,³ and M. Beregovsky¹

¹Department of Electrical Engineering, Technion, Haifa, Israel, 32000

²Department of Material Engineering, Technion, Haifa, Israel, 32000

³IBM T. J. Watson Research Center, Yorktown Heights, New York 10598, USA

(Received 26 December 2010; accepted 9 March 2011; published online 2 May 2011)

The common practice for nickel silicide formation in silicon nanowires (SiNWs) relies on axial growth of silicide along the wire that is initiated from nickel reservoirs at the source and drain contacts. In the present work the silicide intrusions were studied for various parameters including wire diameter (25–50 nm), annealing time (15–120 s), annealing temperature (300–440 °C), and the quality of the initial Ni/Si interface. The silicide formation was investigated by high-resolution scanning electron microscopy, high-resolution transmission electron microscopy (TEM), and atomic force microscopy. The main part of the intrusion formed at 420 °C consists of monosilicide NiSi, as was confirmed by energy dispersive spectroscopy STEM, selected area diffraction TEM, and electrical resistance measurements of fully silicided SiNWs. The kinetics of nickel silicide axial growth in the SiNWs was analyzed in the framework of a diffusion model through constrictions. The model calculates the time dependence of the intrusion length, L , and predicts crossover from linear to square root time dependency for different wire parameters, as confirmed by the experimental data. © 2011 American Institute of Physics. [doi:10.1063/1.3574650]

I. INTRODUCTION

In the last few years field-effect transistors (FETs) based on nickel silicide/Si nanowire (NW) heterostructures in which the source-drain contacts were defined by the metallic nickel silicide NW regions have become an appealing approach for integration of nanoelectronics with CMOS technology.^{1–6} However, precise control of the dimensions of the silicide NW regions is challenging. The kinetics of nickel silicide growth in silicon nanowires (SiNWs) varies substantially according to different studies. For example, linear time dependencies with growth rates of 0.01–0.1 nm/s at 500 °C–650 °C were found by Lu *et al.*³ and Hu *et al.*,⁴ while growth rates of ~ 1 nm/s at 400 °C and ~ 4 nm/s at 450 °C were reported by Dellas *et al.*,⁷ and ~ 15 nm/s at 550 °C by Lin *et al.*⁸ Such differences can be explained by different conditions at the Ni/Si contact area, by different diffusivity of Ni through the nickel silicide phase, or by different phase transformation rates at the NiSi/Si interface (reaction-controlled process).

In order to elucidate the main factors influencing silicide growth rates, nickel silicide/silicon contacts were formed using thermally activated axial intrusion of nickel silicides into the SiNW from e-beam lithography Ni reservoirs located at both ends of the nanowires. Different native oxide layers were grown on the Ni/Si contact area by exposing the SiNW surface to ambient conditions for different delay times (5–30 min) after buffered oxide etch (BOE), and before the metallization step. These oxide layers hamper the diffusion of Ni atoms from their reservoir to the SiNW and, as a result, affect the growth rate of the silicide phase.

II. EXPERIMENTAL DETAILS

The silicon nanowires were synthesized by the vapor-liquid-solid (VLS) method in an ultrahigh vacuum chemical vapor deposition (UHV-CVD) chamber, with silane as the silicon precursor and gold as the catalyst.^{9–11} Two kinds of nanowires were grown: unintentionally doped and lightly p-doped with diborane precursor. The growth temperature was 420 °C. A 2 nm thick gold film that was deposited on a Si (111) substrate was used to form gold catalyst droplets by agglomerating when annealed at 450 °C for 10 min prior to initiation of the growth. The nanowires were grown in $\langle 112 \rangle$, $\langle 110 \rangle$, and $\langle 111 \rangle$ directions with typical diameters of 35–60 nm, 25–40 nm, and above 50 nm respectively, as was confirmed by TEM analysis. The gold catalyst was removed from the nanowire tip by etching the nanowires in a commercial gold etchant (a KI – I₂ based solution). Part of the SiNWs were oxidized in a CVD reactor at 700 °C for 90 min in oxygen atmosphere with flow rate of 200 sccm and pressure of 1 atm.

The SiNWs were randomly dispensed from an ethanol suspension onto Si₃N₄/Si substrate and e-beam lithography was executed to pattern the metal source/drain nickel contacts. Metallic Ni/Au electrodes for the source/drain contacts were deposited by e-beam evaporation. Before metal deposition, a 10 s etch in 1:6 buffered oxide etch (BOE) was performed to remove the thermal or native oxide of the SiNWs in the contact area region. The samples were loaded into the e-beam evaporation system within different delay times, from 5 to 30 min after the BOE, in order to form different barriers of oxide layers in the contact area. The process was done within our clean room facilities where the humidity conditions are kept constant. Metallic electrodes were

^{a)}Author to whom correspondence should be addressed. Electronic mail: yuvaly@ee.technion.ac.il.

deposited by evaporation with a base pressure of 2×10^{-7} Torr. Excess metal was removed by a standard lift-off technique immediately after the wafer was removed from the vacuum chamber. The prepared SiNW/Ni/Au specimens had 140 nm thick Ni layer capped with 20 nm Au. We verified with control samples that the thin gold layer on top of the thick nickel layer does not affect the nickel silicide growth process.

In order to form the nickel silicide/silicon contacts, the samples were inserted into a rapid thermal annealing (RTA) apparatus with a nitrogen atmosphere at different temperatures and times up to 120 s. Series of subsequent annealings with ramp rate of $1^\circ\text{C}/\text{s}$ were performed for different times, from 15 s up to 120 s (usually up to full silicidation) and temperatures (420°C and 440°C). After every annealing step, the silicide intrusions were investigated by high resolution scanning electron microscopy (HRSEM) and atomic force microscopy (AFM).

III. EXPERIMENTAL RESULTS

The kinetics of nickel silicide phase along different SiNWs with native or thermal oxide was investigated at 420°C and 440°C . Typical Ni-silicide intrusion segments during subsequent RTAs of the SiNW sample with native and thermal grown oxide shell are shown in Figs. 1 and 2, respectively. In order to identify the nickel silicide phase of the intrusion adjacent to the silicon part of the wire, a thin lamella was cut from the silicide segment using a focused ion beam (FIB) in a direction perpendicular to the wire longitudinal axis [see Fig. 3(a)]. Transmission electron microscopy (TEM) and energy dispersive spectroscopy (EDS) analysis revealed that the main part of the intrusion segment is the NiSi phase as depicted in Figs. 3(b) and 3(c). The thin NW segment adjacent to the Ni electrode, as depicted in Fig. 3(a), is a consequence of oxide stripping during electrodes deposition. However, in some wires there is more than one phase and the nickel silicide intrusion is composed

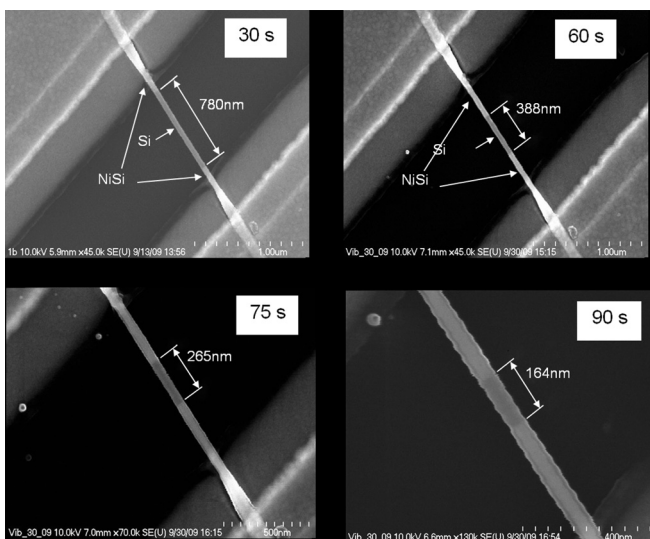


FIG. 1. HRSEM micrographs of SiNWs (with native oxide shell) with Ni-silicide intrusions formed during rapid thermal annealing (RTA) for different times at 420°C .

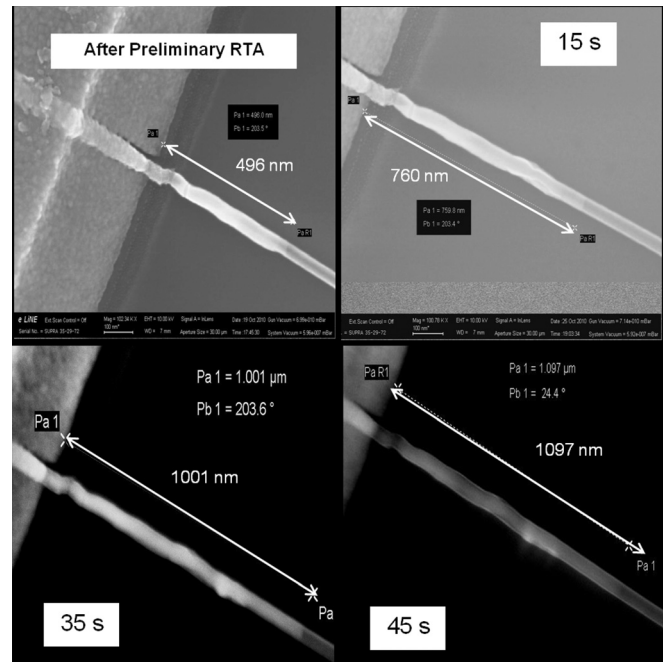


FIG. 2. HRSEM micrographs of SiNWs (with thermal grown oxide shell) with Ni-silicide intrusions formed during rapid thermal annealing (RTA) for different times at 440°C . Clearly one can notice the two silicide phases that were formed along the silicon wire.

from at least two series parts (see Fig. 2), a nickel-rich silicide Ni_{1+x}Si ($x \geq 0$) that is adjacent to the Ni reservoirs, and nickel monosilicide (NiSi) far from the contacts (Figs. 1 and 2). Usually, the nickel-rich phase is wider than the NiSi phase and can be easily detected by AFM analysis. The different phases have different Ni diffusivities and may affect the silicide growth along the wire.

The silicide intrusion growth rate depends on the sample preparation procedure. The longer the exposure time of the sample to an ambient condition (after BOE and before loading into the e-beam evaporation system) the lower the anticipated silicide intrusion growth rate. For short exposure times (≤ 5 min) the evolution of the intrusion length with time is well described by the square root time dependence,

$$L^2(t) - L_0^2 = Dt, \quad (1)$$

as presented in Figs. 4 and 5 for temperatures of 420°C and 440°C , respectively. $L(t)$ is the nickel silicide intrusion length after time t of RTA, L_0 is the initial silicide intrusion length formed by previous annealing steps at different temperatures, and D is the diffusion coefficient, which depends mainly on activation energy and temperature. Later, we describe which diffusion process is the dominant one in the reported study, and explain the origin for the scattering of the growth rate for the different wires. From RTA analysis at different temperatures¹² we extract the activation energy of $E_a = 1.7 \pm 0.15$ eV, which is in good agreement with other studies.^{3,7} The initial growth rate can be defined as $v_{in} = \lim_{t \rightarrow 0} L/dt = D/2L(t)$, and its maximum is found to be 7.9 nm/s at 420°C , and 21.8 nm/sec at 440°C . To the best of our knowledge these initial growth rates are the largest that were published so far, and it can be attributed to the fact that the Ni evaporation was done on

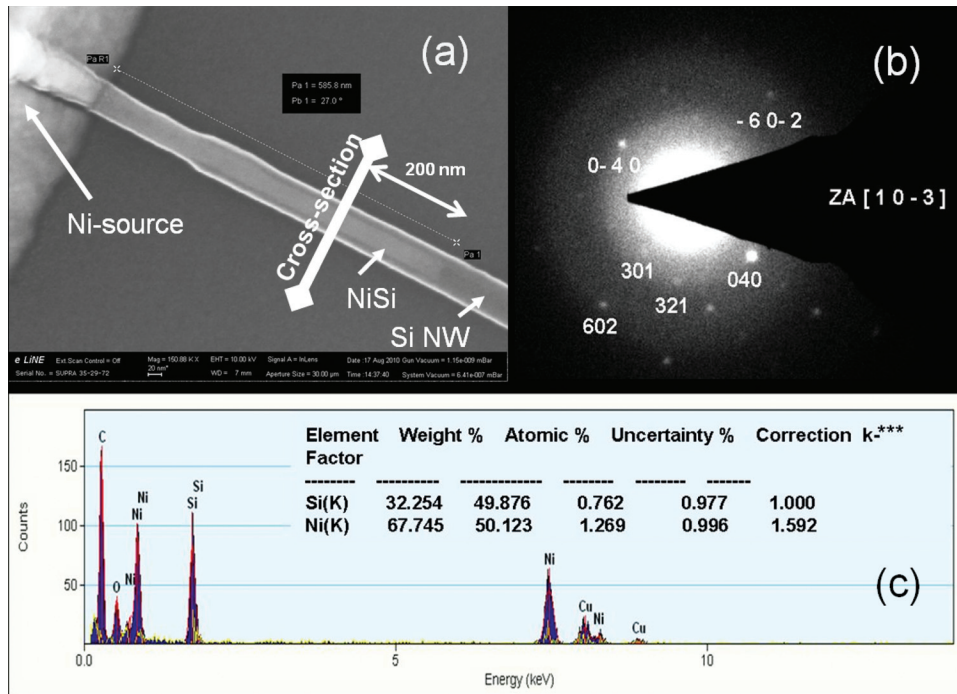


FIG. 3. (Color online) (a) HRSEM image of SiNW with NiSi intrusion formed at 420 °C for 120 s (b) Diffraction pattern from cross-sectional specimen reveals the NiSi phase (c) STEM EDS from the cross-sectional specimen.

rotating stage in which the deposited metal surrounds the wire from almost all directions. Comparable initial silicide growth rate (~15 nm/s at 550 °C) with square root time dependence was recently reported by Lin *et al.*⁸

However, for longer delay times between the etching step and the nickel evaporation (15–30 min) different time dependencies of the silicide intrusion length were observed. At the extreme case linear time behavior was found, as depicted in Figs. 6 and 7, and the growth rate decreases down to ~1 nm/s at 420 °C, and ~6 nm/s at 440 °C.

IV. MODEL OF NICKEL SILICIDE GROWTH IN SINWS

From the experimental data it is clearly seen that the growth rate of NiSi depends dramatically on the quality of the nickel/silicon interface, hence, it is important to include

the role of this interface within any model that attempts to describe silicide formation along SiNWs. Such a possible model for the growth is described below. It is controlled by three sequential processes: (1) transition of Ni atoms from the Ni reservoir to the silicon or the nickel silicide surface; (2) diffusion transport of these Ni atoms from the contact area to the Si/nickel silicide interface; (3) reaction of Ni atoms with Si at the Si/silicide interface resulted in the nickel silicide formation (see Fig. 8).

The flux of Ni atoms from the reservoir across the contact layer of thickness *h* is proportional to the contact area, *S*_{con}, and is given by

$$J_{con} = D_{tr} \frac{(C_{res} - C_0)}{\Omega h} S_{con}, \tag{2}$$

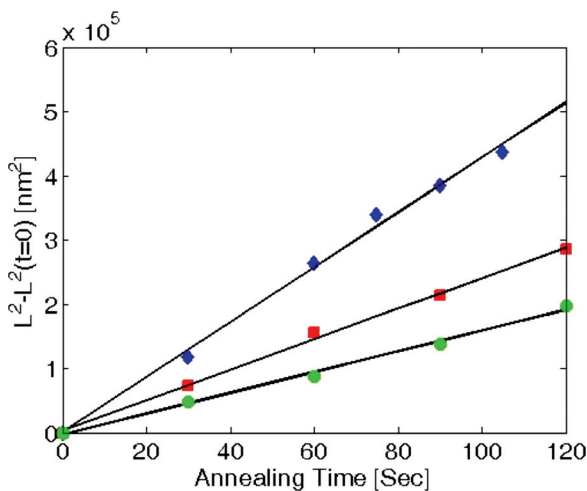


FIG. 4. (Color online) The Ni-silicide intrusion length square versus annealing time at 420 °C for different SiNWs. Diamonds are for the native oxide shell, and squares and circles for ~7.5 nm thick thermal oxide shells. Black lines are best fit according to Eq. (1).

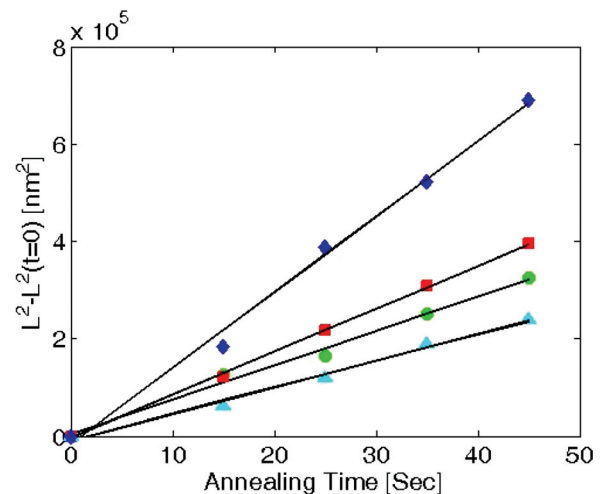


FIG. 5. (Color online) The Ni-silicide intrusion length square versus annealing time at 440 °C for different SiNWs. All the wires have ~5 nm thick thermal oxide shells. Colored symbols represent experimental data and black lines are best fit according to Eq. (1).

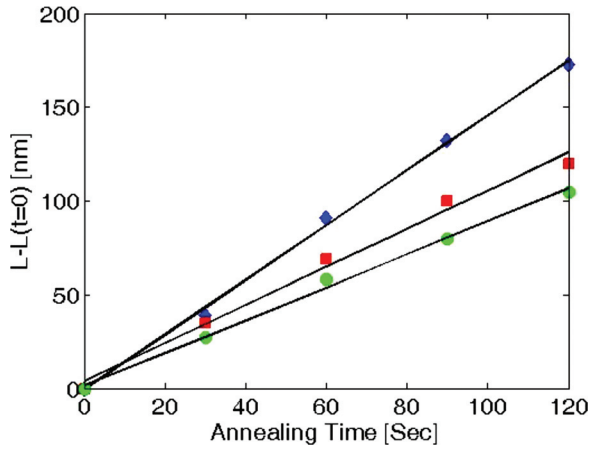


FIG. 6. (Color online) The Ni-silicide intrusion length versus annealing time at 420°C for different SiNWs. All the wires have ~ 5 nm thick thermal oxide shells. Colored symbols represent experimental data and black lines are best fit to linear time dependence.

where D_{tr} is the diffusion coefficient of Ni through the contact layer, C_{res} and C_0 are the dimensionless nickel concentrations in the reservoir and at the silicide interface at the contact area, respectively, and Ω is the atomic volume. The diffusion of Ni atoms along the silicon wire constitutes from bulk and interface diffusion. We assume, according to our previous analysis,¹³ that the surface or silicide/oxide interface diffusion of Ni is the dominant diffusion process. The diffusion flux is proportional to the nickel concentration gradient, and in steady state condition it can be written in the following form:

$$J_{dif} = D_s \frac{(C_0 - C_f)}{\Omega L} 2\pi R \delta, \quad (3)$$

where D_s is the diffusion coefficient of Ni along the nickel silicide surface; and δ is the near-surface diffusion layer width, usually assumed to be about 2–3 atomic layers. L is the silicide intrusion length, and C_f is the dimensionless nickel concentration at the Si/nickel silicide interface. We

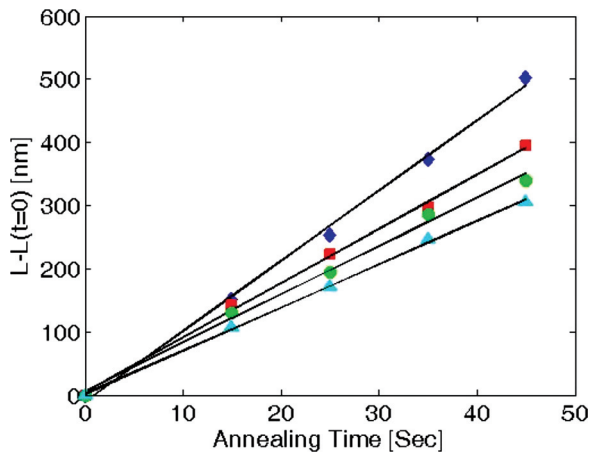


FIG. 7. (Color online) The Ni-silicide intrusion length versus annealing time at 440°C for different SiNWs. All the wires have ~ 5 nm thick thermal oxide shells. Colored symbols represent experimental data and black lines are best fit to linear time dependence.

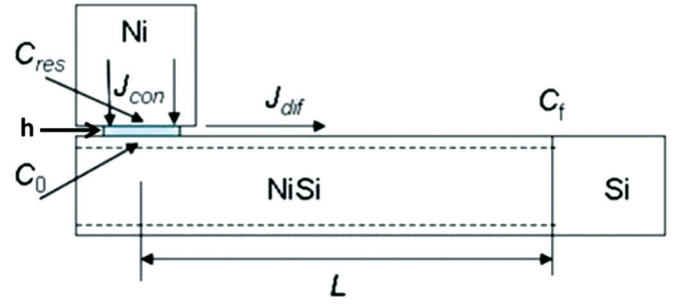


FIG. 8. (Color online) Schematic model for nickel silicide intrusion growth process during thermal annealing.

neglect here Si diffusion, which is much slower than diffusion of Ni at the temperatures under consideration. Moreover, the model was simplified for the case of the single silicide phase, in order to demonstrate the influence of contact layer quality on silicide growth. In reality, more than a single silicide phase may occur and the model can be easily extended to the case of several silicide segments that form simultaneously in steady state condition. Such analysis for the case of two kinds of silicide formation is described in the Appendix, and proves that the simplified model is sufficient for describing the experimental data, with renormalization of the effective growth parameters.

Returning to the single silicide phase growth model, from the mass balance condition, $J_{con} = J_{dif}$, one extracts the nickel concentration at the contact area, C_0 ,

$$C_0 = \frac{C_f + C_{res} \left(\frac{LS_{con} D_{tr}}{h S_R D_S} \right)}{1 + \frac{LS_{con} D_{tr}}{h S_R D_S}}, \quad (4)$$

where $S_R = 2\pi R \delta$, and after plugging C_0 into the diffusion flux equation [Eq. (3)] one finds

$$J_{dif} = \frac{D_s}{\Omega L + h(D_s S_R / D_{tr} S_{con})} S_R (C_{res} - C_f). \quad (5)$$

Since we are interested in the growth rate of the silicide phase, it can be found from comparing the total Ni atoms that arrive at the Si/silicide interface in a given time interval, $dN_1 = J_{dif} dt$, to the number of Ni atoms that form the silicide phase in the narrow disk of radius R and length dL , $dN_2 = \pi R^2 dL / 2\Omega$, where the factor 2 comes from the fact that only half of the atoms in the NiSi phase are nickel. The silicide growth rate, $v(t) = dL/dt$, can be extracted from the condition $dN_1 = dN_2$, and is found to be

$$v(t) = \frac{dL}{dt} = J_{dif} \frac{2\Omega}{\pi R^2} = D_s \frac{C_{res} - C_f}{L + h(D_s S_R / D_{tr} S_{con})} \frac{4\delta}{R}. \quad (6)$$

Integration of Eq. (6) from $t=0$ up to t , with the boundary condition $L(t=0) = L_0$, yields the time dependence of the intrusion length:

$$L(t) = A \left(\sqrt{t + (\sqrt{\tau} + L_0/A)^2} - \sqrt{\tau} \right), \quad (7)$$

where $A = \sqrt{8D_s(C_{res} - C_f)\delta/R}$, L_0 is the initial silicide intrusion length formed by previous annealing steps at different temperatures, and $\tau = \bar{g}^2\tau_R$ is the transition time from linear to square root behavior. \bar{g} is geometric factor which is given by

$$\bar{g} = \frac{S_R h}{S_{con} \delta}, \quad (8)$$

and

$$\tau_R = \frac{D_s R \delta}{8D_{tr}^2(C_{res} - C_f)}. \quad (9)$$

Eq. (7) reveals two limiting behavior. For short time, where $t \ll \tau$, the silicide intrusion length grows linearly with time:

$$L - L_0 \approx \frac{S_{con} \delta}{S_R h} (C_{res} - C_f) \frac{4D_{tr}t}{R} = \frac{4D_{tr}t C_{res} - C_f}{R \bar{g}}. \quad (10)$$

In the opposite case, where $t \gg \tau$, the growth law is square root:

$$L^2 - L_0^2 \approx 8D_s t (C_{res} - C_f) \frac{\delta}{R}. \quad (11)$$

For a conventional situation, where the diffusion of Ni atoms from the Ni reservoir to the silicon wire is much faster than the diffusion along the wire itself, τ is very small and the expected square root behavior is predicted. Nevertheless, differences between the silicide growth rates are still possible because of variability in $D_s(C_{res} - C_f)\delta/R$, as seen in Figs. 4 and 5. However, for a poor quality interface, whether because of small contact area, S_{con} , or thick interface, h , or poor diffusivity across the interface, D_{tr} , τ increases and the linear regime lasts for a longer time. In the extreme case when

$$\frac{S_R}{S_{con}} \gg \frac{D_{tr} L_{ini}}{D_s h}, \quad (12)$$

where L_{ini} is the initial silicon channel length, the growth regime could be linear up to full silicidation.

V. ANALYSIS OF EXPERIMENTAL RESULTS

Next, we analyze the two sets of data, L versus t , for the two annealing temperatures, 420 °C and 440 °C, and examine their agreement with expression (7). L_0 is measured from the experimental data, and two fitting parameters, A , and τ should be determined. τ is specific for each wire. It depends on the Ni contact area (geometric factor), on the diffusion across the Ni/nickel silicide contact, on the interface quality, on the Ni concentration difference, and diffusion along the wire itself. The situation is quite different for the second parameter, A . For SiNWs with similar δ/R and $C_{res} - C_f$, A is expected to be the same for a given temperature, and should have Arrhenius temperature behavior originating from the Ni diffusion coefficient, D_s . Specifically, since in previous studies^{3,7,12} the diffusion activation energy was found to be $E_a \sim 1.7\text{eV}$, $A(440^\circ\text{C})/A(420^\circ\text{C}) \sim 1.48$, and only one

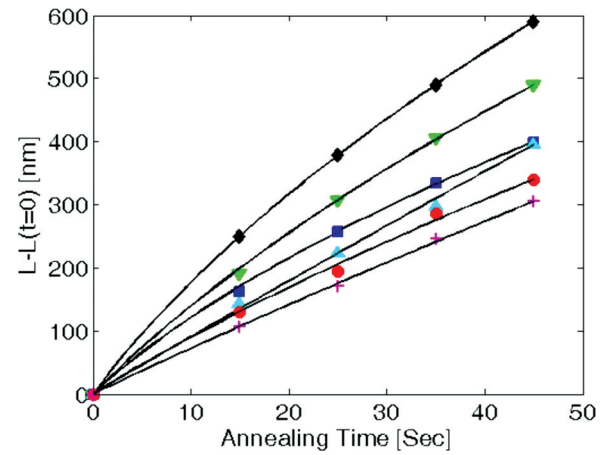


FIG. 9. (Color online) The Ni-silicide intrusion length versus annealing time at 420 °C for different SiNWs. Black lines are best fit according to Eq. (7).

single A (besides τ for each wire) should be found. However, in reality, the situation is more subtle. As was emphasized before, some part of the nickel silicide intrusion is composed of at least two series parts, a nickel-rich silicide Ni_{1+x}Si ($x \geq 0$) and nickel monosilicide (NiSi), with different diffusivities and different activation energies. From the analysis in the Appendix one finds from Eq. (24) that indeed A depends on the diffusion coefficients of both silicide phases, and not on that of the monosilicide alone. Moreover, the Ni-rich phase imposes strain on the wire and, as a consequence, affects the diffusion coefficients of the two phases as well. Eqs. (23) and (24) describe the silicide kinetics for the case of two silicide phases. In a subsequent paper we will report on the influence of such strain on the monosilicide kinetics and growth. In addition, some wires could have different $C_{res} - C_f$ or δ and, hence, different A . As a result out, of 16 wires that are presented in this study, 4 wires from the two data sets have the same A (up to Arrhenius factor), but the rest have different A . Figures 9 and 10 present the two data sets, and the agreement with Eq. (7) (continuous lines) is excellent.

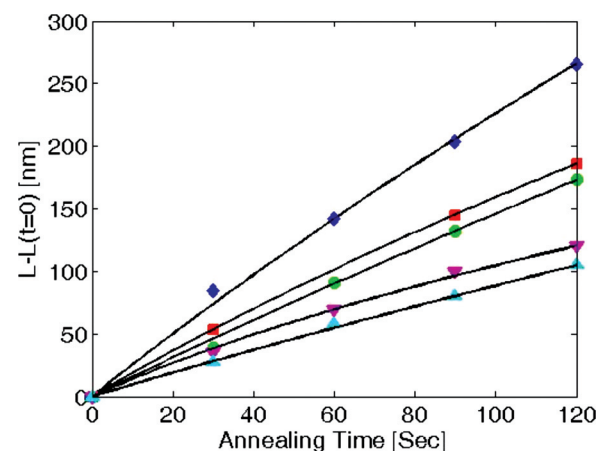


FIG. 10. (Color online) The Ni-silicide intrusion length versus annealing time at 440 °C for different SiNWs. Black lines are best fit according to Eq. (7).

TABLE I. L_0 , A , and τ for the 16 SiNWs under study. Wires N1–T8 were annealed at 420 °C, and wires T11–T18 at 440 °C.

	N1	T1	T2	T3	T4	T5	T6	T7	T8	T11	T12	T13	T14	T16	T17	T18
L_0 (nm)	271	238	238	136	111	111	76	89	78	506	412	296	207	189	177	238
A (nm/ \sqrt{s})	67	48.8	75	39.4	76	32.2	19.6	32.8	132.6	145	132.6	109	145	307.7	111	164
τ (s)	0.13	0	84	47.4	233	82.2	8	209.5	1.3	0	1.3	2.13	52.9	264.8	16.2	94.6

Table I summarizes the results for the fitting parameters, A and τ , for 16 SiNWs that were tested during this study. For SiNWs T2 and T4 (diamonds and circles in Fig. 9), the A 's are almost the same, and by multiplying by the appropriate Arrhenius factor, 1.48, one obtains ~ 110 which is very close to the A values of wires T13 and T17 (diamonds and circles in Fig. 10). However, for others wires, there is a spread of the possible values of A . As expected, the distribution of τ is very broad, and reflects the two main physical processes of silicide growth along the wire; a) diffusion across the Ni reservoir/silicon interface b) diffusion along the silicon wire.

The above results suggest that by appropriate scaling of the experimental data, all the data should collapse to a single line. Subtracting from Eq. (7) L_0 , dividing by L_0 , and extracting $\sqrt{\tau}$ from the RHS square root yield

$$\frac{L}{L_0} = \frac{A\sqrt{\tau}}{L_0} \left(\sqrt{\frac{t}{\tau} + \left(1 + \frac{L_0}{A\sqrt{\tau}}\right)^2} - 1 \right) - 1, \quad (13)$$

and after simple algebra transforms into

$$F \equiv \frac{L^2}{A^2\tau} \left(1 + \frac{2A\sqrt{\tau}}{L} + \frac{2L_0}{L} \right) = \frac{t}{\tau}. \quad (14)$$

Figure 11 presents F as defined in Eq. (14) versus t/τ for the two sets of data (blue diamonds, and red circles stand for 420 °C and 440 °C data sets, respectively). It is clearly evident that all the data, in the main and inset panels, collapse to a single line (dot-dash line), with slope equal to 1 as predicted by Eq. (14). The scaling x-axis, t/τ , spans broad

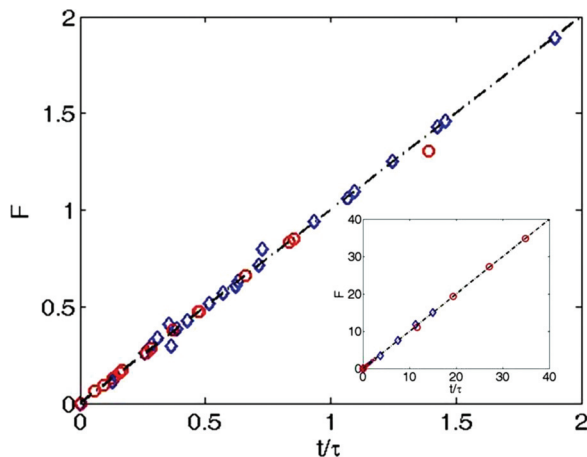


FIG. 11. (Color online) F as defined in Eq. (14) versus t/τ for the two sets of data. Diamonds and circles stand for 420 °C and 440 °C data sets, respectively. Dot-dash line presents straight line with slope equal to 1. Inset: The same as the main panel, but with larger range.

range of values and reflects the transition from linear to square root silicide growth dependence. Eq. (14) signifies three dimensionless parameters that govern the growth process: t/τ , L_0/L , and $L/(A\sqrt{\tau})$. After plugging the definition of A and τ one finds

$$\frac{L}{A\sqrt{\tau}} = \frac{LD_{tr}}{\delta D_s}. \quad (15)$$

For high transparency of the Ni-reservoir/silicon interface, i.e., $D_{tr} \gg D_s$, the process will be controlled by the diffusion along the silicon wire, but for a poor interface, the supply rate of Ni atoms can be affected and, hence, modify the growth kinetics.

VI. DISCUSSION

A very limited data set on time and temperature dependencies of nickel silicide growth in SiNWs are available in the literature. Huge variation of rates, sometimes about 3 orders of magnitude at the same temperature, points to the substantial influence of contact area on the silicide growth rate. It is worth noting that phase transformation rate at the silicide/Si interface could not be a factor controlling the total process rate, since it does not vary significantly at a given temperature. On the other hand, supply of Ni atoms may differ significantly depending on the initial conditions at the Ni/Si and Ni/silicide contact area. As it was demonstrated above, the maximum growth rate corresponds to a good contact area where the growth is limited only by diffusion of Ni along the silicide outer surface or along the silicide/oxide interface toward the silicide/Si interface. This is a diffusion-controlled process providing square root time dependence of silicide intrusion length. However, when supply of nickel atoms is hampered, for example, due to oxide layer at the Ni/Si contact area, the geometry factor, \bar{g} , is large, and the growth law within the experimental annealing times, $t < \tau$, is close to linear one. In such situations, the growth rate is inversely proportional to the geometry factor and can vary in a wide range. Indeed, the distribution of the experimental values of τ is very broad, and strengthens our assumptions. Assuming, for example, $D_{tr} = D_s$, $C_{res} = 1$, $C_f = 0.5$, $R/\delta = 30$, and $h = 2\delta$, one finds

$$\tau = \frac{30\delta^2}{D_s} \left(\frac{S_R}{S_{con}} \right)^2. \quad (16)$$

For typical $D_s = 10^{-11} \text{ cm}^2/\text{s}$, $\delta = 0.5 \text{ nm}$, and $S_R/S_{con} = 10$, Eq. (16) yields $\tau = 0.75 \text{ s}$, and the growth should have square root behavior. However, for $S_R/S_{con} = 100$, τ is already 75s. The smaller the effective contact area, the longer the linear

regime of the silicide intrusion growth process will be. In the case of point contact between the Ni and the SiNW, the linear regime is apparently maintained along all the annealing process until full silicidation of the entire wire is achieved.

In previous studies^{1,3,7} researchers found reciprocal dependence of the axial silicide growth rate on wire diameter, i.e., for thinner wires the growth rate is higher and vice versa. This dependence was found in the present study as well, however, unfortunately, limited available data do not allow us to reveal this dependence quantitatively. In most “near-linear” cases it is certainly stronger than $L^2 \sim 1/R$ corresponding to diffusion controlled growth, Eq. (11), and very close to $L \sim 1/R^2$, corresponding to Eq. (10). This result suggests that the rate-limiting step is indeed transport of Ni through the porous SiO₂ shell. However, in the general case, the silicide growth is determined by both the Ni transfer through the oxide in the contact area and by diffusion of Ni along the silicide intrusion to the silicide/Si interface. Linear and square root dependencies are two limiting cases of more general behavior that is described by Eq. (7) and verified experimentally in Figs. 10 and 11.

VII. CONCLUSION

This article reports on experimental and theoretical studies of nickel silicide formation in SiNWs. Nickel silicide was formed during a thermal annealing process, and measured using AFM, HRSEM, and HRTEM. A theoretical model was developed and excellent agreement between theory and experiment was obtained. It was found that the growth of nickel silicide intrusions in SiNWs is controlled by: (1) diffusion of Ni atoms from the Ni reservoir to the silicon or the nickel silicide surface; and (2) diffusion transport of these Ni atoms from the contact area to the Si/nickel silicide interface. General time dependence can be found and the transition time from linear to square root behaviors depends on nickel diffusivities and a geometry factor that was introduced in the model developed. For sufficiently high geometry factor, or poor diffusivity of Ni atoms from their reservoir to the silicon wire, the growth regime can be linear up to full silicidation of the entire wire.

ACKNOWLEDGMENTS

We thank the Russell Berrie Nanotechnology Institute, and the Israeli Ministry of Industry, Trade & Labor via MAGNET program (ALPHA consortium) for support.

APPENDIX: TWO PHASES MODEL

The model of silicide growth can be extended to more than one silicide phase. In this appendix we derive the analogous expression for Eq. (7) for the case of two kinds of silicide that grow simultaneously along the silicon wire. Segment 1 is adjacent to the Ni reservoir and usually consists of nickel-rich silicide, Ni_{1+x}Si, where 1 + x is the fraction of Ni in the rich phase. Segment 2 is adjacent to the silicon part

of the wire and is usually NiSi. Since the two phases progress simultaneously the chemical reaction at the interface between the two silicide phases can be described by the following relation: $x \times \text{Ni} + \text{NiSi} \rightarrow \text{Ni}_{1+x}\text{Si}$. At the monosilicide/silicon interface the chemical reaction is formulated by $\text{Ni} + \text{Si} \rightarrow \text{NiSi}$. The two segments are described by two lengths, $L_1(t)$, and $L_2(t)$, have different interface diffusion coefficients, D_{s1} and D_{s2} , different radii, R_1 and R_2 , different atomic volumes, Ω_1 and Ω_2 , and different near-surface diffusion layer widths, δ_1 , and δ_2 . The flux of Ni atoms from the Ni reservoir to the wire, J_{con} , is given as previously by Eq. (2), where Ω is the near-surface atomic volume. The fluxes of Ni atoms along phases 1 and 2 are written as

$$J_{\text{dif}}(1) = D_{s1} \frac{(C_0 - C_f)}{\Omega(L_1 + L_2)} 2\pi R_1 \delta_1, \quad (\text{A1})$$

$$J_{\text{dif}}(2) = D_{s2} \frac{(C_0 - C_f)}{\Omega(L_1 + L_2)} 2\pi R_2 \delta_2, \quad (\text{A2})$$

where we assume that the nickel concentration changes linearly along the silicide segment (1 and 2) and C_0 (C_f) is the dimensionless nickel concentration in the beginning (end) of the two silicide phases. As before, from the mass balance equation, $J_{\text{con}} = J_{\text{dif}}(1)$, one derives C_0 ,

$$C_0 = \frac{C_f + C_{\text{res}} \left(\frac{(L_1 + L_2) S_{\text{con}} D_{\text{tr}}}{h S_{R1} D_{s1}} \right)}{1 + \frac{(L_1 + L_2) S_{\text{con}} D_{\text{tr}}}{h S_{R1} D_{s1}}}, \quad (\text{A3})$$

$$= \frac{C_f + C_{\text{res}} \left(\frac{(L_1 + L_2) b}{h} \right)}{1 + \frac{(L_1 + L_2) b}{h}},$$

where $S_{R1} = 2\pi R_1 \delta_1$, and $b = S_{\text{con}}/S_{R1} D_{\text{tr}}/D_{s1}$. Next, we need to formulate the growth rate of each phase separately. The diffusion flux of Ni in segment 1 provides the Ni supply for the growth of phase 1 as well as 2, therefore, the mass balance equation across the two silicide phases can be described by the following expression

$$J_{\text{dif}}(1) = J_{\text{dif}}(2) + \frac{dL_1(t)}{dt} \frac{\pi R_1^2 x}{\Omega_1(2+x)}, \quad (\text{A4})$$

where the additional $x/(2+x)$ originates from the relative fraction of Ni within the unit cell of the Ni-rich phase. Phase 2 undergoes two competing processes. On one hand, the diffusion flux, $J_{\text{dif}}(2)$, increases its length by $\propto d\tilde{L}_2(t)$ within interval time dt , but on the other hand, it decreases by $\propto dL_1(t)$ as a consequence of the transformation from NiSi to Ni_{1+x}Si. Thus, the total growth rate of phase 2 is given by

$$\frac{dL_2(t)}{dt} = \frac{d\tilde{L}_2(t)}{dt} - \frac{dL_1(t)}{dt} \frac{2}{2+x} \frac{R_1^2 \Omega_2}{R_2^2 \Omega_1}, \quad (\text{A5})$$

where dL_1/dt is extracted from Eq. (A4), and

$$\frac{d\tilde{L}_2(t)}{dt} = \frac{2\Omega_2 J_{dif}(2)}{\pi R_2^2}. \quad (\text{A6})$$

Adding $dL_1/dt + dL_2/dt$, and plugging in C_0 from Eq. (A3) yields

$$\begin{aligned} \frac{d}{dt}(L_1 + L_2) &= \frac{4D_{s2}\delta_2\Omega_2}{R_2h} \frac{b(C_{res} - C_f)}{\Omega} \frac{1}{1 + b\frac{(L_1 + L_2)}{h}} \\ &\times \left(1 + \frac{1}{x} \left(\frac{\Omega_1}{\Omega_2} \frac{2 + xR_2^2}{2R_1^2} - 1 \right) \left(\frac{D_{s1}S_1}{D_{s2}S_2} - 1 \right) \right). \end{aligned} \quad (\text{A7})$$

After integration of the last equation and using the boundary condition $L_0 = L_1(t=0) + L_2(t=0)$, one finds the quadratic equation for $L(t) = L_1(t) + L_2(t)$ with the following solution

$$L(t) = A \left(\sqrt{t + (\sqrt{\tau} + L_0/A)^2} - \sqrt{\tau} \right), \quad (\text{A8})$$

where

$$A = \sqrt{8D_{s2}(C_{res} - C_f) \frac{\delta_2\Omega_2}{R_2} \Omega} (1 + \alpha), \quad (\text{A9})$$

$$\alpha = \left(1 + \frac{1}{x} \left(\frac{\Omega_1}{\Omega_2} \frac{2 + xR_2^2}{2R_1^2} - 1 \right) \left(\frac{D_{s1}S_1}{D_{s2}S_2} - 1 \right) \right), \quad (\text{A10})$$

L_0 is the initial silicide intrusion length formed by previous annealing steps at different temperatures, and $\tau = \bar{g}^2 \tau_R$ is the transition time from linear to square root behavior. \bar{g} is geometric factor which is given by

$$\bar{g} = \frac{S_{R1}h}{S_{con}\delta_2}, \quad (\text{A11})$$

and

$$\tau_R = \frac{D_{s1}^2 R_2 \delta_2 \Omega}{8D_{s2} D_{ir}^2 \Omega_2 (C_{res} - C_f) (1 + \alpha)}. \quad (\text{A12})$$

Eq. (A8) is identical to Eq. (7), and Eqs. (A10), (A11), and (A12) coincide with the expression for A , and Eqs. (8) and (9) for the single silicide phase. These results confirm our single-phase model that was presented in the main text.

- ¹J. Appenzeller, J. Knoch, E. Tutuc, M. Reuter, and S. Guha, International Electron Devices Meeting (2006).
- ²W. M. Weber, L. Geelhaar, A. P. Graham, E. Unger, G. S. Duesberg, M. Liebau, W. Pamler, C. Cheze, H. Riechert, P. Lugli, and F. Kreupl, *Nano Lett.* **6**, 2660 (2006).
- ³K.-C. Lu, W.-W. Wu, H.-W. Wu, C. M. Tanner, J. P. Chang, L. J. Chen, and K. N. Tu, *Nano Lett.* **7**, 2389 (2007).
- ⁴Y. Hu, J. Xiang, G. Liang, H. Yan, and C. M. Lieber, *Nano Lett.* **8**, 925 (2008).
- ⁵W. Weber, L. Geelhaar, E. Unger, C. Chèze, F. Kreupl, H. Riechert, and P. Lugli, *Phys. Status Solidi B* **244**, 4170 (2007).
- ⁶K. Sarpatwari, N. S. Dellas, O. O. Awadelkarim, and S. E. Mohny, *Solid-State Electron.* **54**, 689 (2010).
- ⁷N. S. Dellas, B. Z. Liu, S. M. Eichfeld, C. M. Eichfeld, T. S. Mayer, and S. E. Mohny, *J. Appl. Phys.* **105**, 094309 (2009).
- ⁸Y. C. Lin, Y. Chen, D. Xu, and Y. Huang, *Nano Lett.* **10**, 4721 (2010).
- ⁹R. S. Wagner and W. C. Ellis, *Appl. Phys. Lett.* **4**, 89 (1964).
- ¹⁰J. Westwater, D. P. Gosain, S. Tomiya, S. Usui, and H. Ruda, *J. Vac. Sci. Technol. B* **15**, 554 (1997).
- ¹¹A. M. Morales and C. M. Lieber, *Science* **279**, 208 (1998).
- ¹²Y. E. Yaish, M. Beregovsky, G. M. Cohen, and A. Katsman (2011), preprint.
- ¹³A. Katsman, Y. Yaish, E. Rabkin, and M. Beregovsky, *J. Electron. Mater.* **39**, 365 (2010).